Communication-Less Frequency Support from Offshore Wind Farms Connected to HVdc via Diode Rectifiers

Oscar Saborío-Romano, *Student Member*, *IEEE*, Ali Bidadfar, *Member*, *IEEE*, Jayachandra N. Sakamuri, Lorenzo Zeni, *Member*, *IEEE*, Ömer Göksu, Nicolaos A. Cutululis, *Senior Member*, *IEEE*

***Abstract*—Before diode rectifier (DR) technology for connecting offshore wind farms (OWFs) to HVdc is deployed, in-depth studies are needed to assess the actual capabilities of DR-connected OWFs to contribute to the secure operation of the networks linked to them. This study assesses the capability of such an OWF to provide communication-less frequency support (CLFS) to an onshore ac network. It is shown that the HVdc link's offshore terminal direct voltage can be estimated from measurements at the OWF's point of connection with the DR platform. Two different methods are proposed for implementing CLFS in the OWF active power controls. In Method 1, the estimated offshore terminal direct voltage is used for estimating the onshore frequency deviation. In Method 2, the actual offshore terminal direct voltage measurement is used instead. Unique features of the provision of CLFS from OWFs connected to HVdc via DRs are highlighted, and the dynamic and static performance of the CLFS control scheme is compared to that of the communication-based frequency support scheme. To assess the impact of parameter estimation errors on the provision of CLFS, a parametric sensitivity study is presented as well, and recommendations are given to increase accuracy.**

***Index Terms*—Diode-rectifier-based HVdc transmission, frequency support, grid-forming wind turbine control, offshore wind energy integration, primary frequency response**

I. Introduction

EXPLOITING Europe's offshore wind resources further requires the development of electrical infrastructure connecting offshore wind farms (OWFs) and onshore networks. To date, only a few OWFs are connected via HVdc, while the majority export their production through HVac. However, as the distance from shore and OWF size increase and the associated costs decrease, the amount of HVdc-connected OWFs is widely expected to increase.

Since its introduction in 1997, HVdc transmission technology using voltage source (forced-/self-commutated) converters (VSCs), based on insulated-gate bipolar transistors, has developed significantly. VSC-based HVdc transmission (VSC-HVdc) offers advantages such as independent control of active and reactive power, smaller footprints, fast reversibility of active power flow and the (grid-forming) capability to form ac networks, i.e. to control their ac-side voltage magnitude and frequency. Owing to such advantages, the use of VSC-based offshore HVdc terminals has enabled the development of HVdc-connected OWFs with the prevailing grid-following approach to controlling wind turbines (WTs), in which WTs rely on other (grid-forming) units (e.g. VSC-based offshore HVdc terminals) forming their ac network.

Recently suggested as a feasible alternative for connecting OWFs to HVdc, (uncontrolled, line-commutated) diode rectifiers (DRs) have prompted increasing interest from both academia and industry [1]–[6]. DR-based offshore HVdc terminals offer advantages such as higher reliability, lower costs, higher efficiency and smaller footprints [3], [5]. Since diodes are passive devices, however, such offshore HVdc terminals are inherently devoid of the grid-forming capability of VSCs. WTs have therefore been suggested as feasible candidates to take over such responsibility. This entails fundamentally different WT and WF controls, changing their control approach from that of grid-following units to that of grid-forming units [1], [4].

HVdc-connected OWFs and the corresponding HVdc power transmission networks can be required to contribute to the secure operation of the onshore ac networks connected to them by means of e.g. fault ride-through, black start and restoration, rotor angle stability-related control, reactive power/alternating voltage control and active power/frequency control. The capabilities of VSC-HVdc-connected OWFs and the corresponding HVdc power transmission networks to provide such services are well established. In-depth studies are, however, needed to assess the actual capabilities of DR-connected OWFs to contribute in the provision of such services before such technology is deployed [7].

A control strategy for the provision of frequency support (FS) from HVdc-connected WFs was first developed in [8], based on the long-distance communication of the remote ac network's frequency to the WF-side HVdc terminal, hereinafter referred to as *communication-based frequency support* (CBFS). To avoid the need of long-distance communication, communication-less schemes have been subsequently proposed for the provision of FS, hereinafter referred to as *communication-less frequency support* (CLFS), from VSC-HVdc-connected OWFs [9], [10]. The term *communication-less* means, in this context, without long-distance commu-

This work has received funding from the European Union's Horizon 2020 research and innovation programme under grant agreement No 691714.

O. Saborío-Romano, A. Bidadfar, Ö. Göksu and N. A. Cutululis are with the Department of Wind Energy, Technical University of Denmark, Frederiksborgvej 399, 4000 Roskilde, Denmark (e-mail: osro@dtu.dk; abid@dtu.dk; omeg@dtu.dk; niac@dtu.dk).

L. Zeni is with Ørsted Offshore, Nesa Allé 1, 2820 Gentofte, Denmark (e-mail: lorze@orsted.dk).

J. N. Sakamuri is with Vattenfall, Jupitervej 6, 6000 Kolding, Denmark (e-mail: jayachandranaidu.sakamuri@vattenfall.com).

nication, i.e. all quantities needed by each controller can be measured *locally*. For an OWF, *locally* means at its point of connection, which may be extended for DR-connected OWFs to include the DR platform.

The capability of DR-connected OWFs to provide CBFS to onshore ac networks by means of plant-level controls similar to those devised for VSC-connected OWFs has been investigated in [11], using models and grid-forming WT front-end converter (FEC) controls based on those in [1]–[3], and an aggregated representation of the OWF as a single equivalent WT. The analysis has been extended in [12], using more detailed component models based on those in [13], a semi-aggregated representation of the OWF and improved grid-forming WT FEC controls based on those in [6].

To date, CLFS from DR-connected OWFs has only been studied in [14], where supplementary WT controls have been proposed to detect the onshore frequency event via the corresponding change in the magnitude of the voltage in the offshore ac network (clamped to the HVdc network voltage) and change the WT active power output by manipulating the pitch angle once the fluctuation in voltage magnitude surpasses a certain threshold value. The performance of such controls has been illustrated by simulation results corresponding to two operating points very close to each other, not considering the accuracy with regards to the expected changes in WF active power output in response to the changes in the frequency of the onshore ac network. However, since the voltage drop over the DRs varies with the operating point, an accurate provision of such service over the whole operating range of the OWF will inevitably require that:

- such WTs receive information about the operating point (e.g. WF active power or current output) that is not available from measurements local to the WTs, and that
- some parameters of the proposed supplementary WT controls (e.g. voltage magnitude threshold, droop) vary with the operating point.

The main contribution of this work, extending the assessment conducted in [12], is to include the capability of the DR-connected OWF to provide CLFS to an onshore ac network by means of plant-level controls similar to those devised for VSC-connected OWFs. It is shown that the HVdc link's offshore terminal direct voltage can be estimated from measurements at the OWF's point of connection with the DR platform and offline estimation of parameters corresponding to the DR platform. Furthermore, it is shown that the onshore frequency deviation can in turn be estimated from the offshore terminal direct voltage estimation and the coordinated selection of the corresponding droops in the onshore terminal and OWF active power controls.

Two different methods are proposed for implementing CLFS in the WF active power controls. In Method 1, the estimated offshore terminal direct voltage is used for estimating the onshore frequency deviation. In Method 2, the actual offshore terminal direct voltage measurement is used instead.

Through the proposed controls, the OWF modifies its active power output according to the estimation of the onshore frequency deviation. Focus is given to primary frequency response (PFR), based on an active-power-frequency droop,

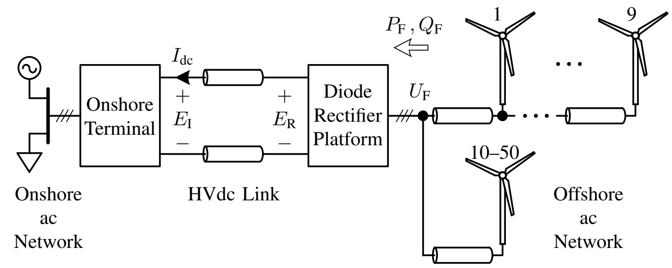

Fig. 1. Overview of the studied system

with the reserves from preventively curtailed operation considered as the source of additional active power during onshore underfrequency events [13]. Unique features of the provision of CLFS from OWFs connected to HVdc via DRs are highlighted, and the dynamic and static performance of the CLFS control scheme is compared to that of the CBFS scheme. To assess the impact of parameter estimation errors on the provision of CLFS, a parametric sensitivity study is presented as well, and recommendations are given to increase the accuracy in the estimation of such parameters.

The rest of the paper is organised as follows. In Section II, the studied system is detailed and the main control algorithms are described. In Section III, the considered cases are described, and corresponding simulation results are presented and discussed. Finally, concluding remarks are made in Section IV.

II. Modelling and Control

Fig. 1 shows an overview of the studied system. The system is based on that described in [7], [13] and consists of one of three $400\,\mathrm{MW}$ OWFs connected to an onshore ac network by means of a $200\,\mathrm{km}$ long $\pm 320\,\mathrm{kV}$ monopolar HVdc link and corresponding onshore HVdc terminal, operating at a third of the rated voltage (i.e. the nominal voltage is approximately $213\,\mathrm{kV}$, and the nominal power is $400\,\mathrm{MW}$). Balanced/symmetric operation is assumed.

A lumped three-phase synchronous machine (SM) with its governor and turbine, and a lumped three-phase load represent the onshore ac network. The share of wind power generation at the connection point is $50\,\%$, i.e. the WF is rated at $400\,\mathrm{MW}$, for a total installed capacity of $800\,\mathrm{MW}$. The offshore HVdc terminal: one of three diode rectifier platforms (one per OWF), consists of two (uncontrolled, line-commutated) diode-based 12-pulse rectifiers (DRs) connected in series, with corresponding reactive power compensation and filter bank on their ac side.

The OWF has 50 type-4 (full-converter) $8\,\mathrm{MW}$ WTs, laid out in 6 strings. The first string, comprised of WTs 1–9 is represented in detail. The other 5 strings, consisting of WTs 10–50, are aggregated into an equivalent $328\,\mathrm{MW}$ WT and corresponding cable equivalent π circuit using the method proposed in [15].

Dynamics in each WT dc link and behind it are not considered, as they are not relevant to the case in question. The corresponding voltage is thus assumed constant, i.e. ideally regulated by the back-end/machine-side converter [7].

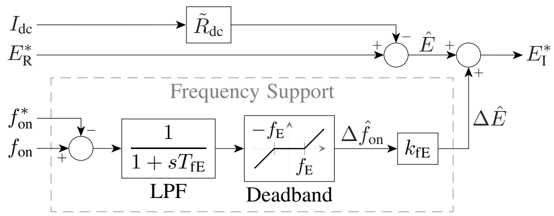

Fig. 2. Onshore terminal outer control loop; parameter values and limits given in Table I

Pulse-width modulation (PWM) is assumed to be done in the linear range, switching effects and any delay due to the implementation of the PWM are neglected, and average value models are used to represent all VSCs (including the VSC-based onshore HVdc terminal). Focus is given to dynamics not faster than the VSC (inner/lower) current control loops, the fastest of which are designed to have a bandwidth of 200 Hz.

A. *Onshore Terminal Control*

The VSC-based onshore HVdc terminal regulates the voltage on its dc terminals, E_{I}, and the reactive power injected into the onshore ac network by means of the controls described in [3]. To study the capability of such an OWF to provide CLFS to an onshore ac network, the onshore terminal controls are extended to include the outer control loop shown in Fig. 2, based on those used in [9], [10], [16] for OWFs connected to HVdc via VSCs. In such loop, the base direct voltage reference, $\hat{E}$, is determined by subtracting the estimated voltage drop on the HVdc link from the offshore terminal direct voltage reference, E_{R}^{*}, which is set to the nominal value. The voltage drop on the HVdc link is calculated using the onshore terminal current measurement, I_{dc}, and the estimated HVdc link resistance, $\tilde{R}_{\mathrm{dc}}$.

When CLFS is provided, $\hat{E}$ is modified by means of an additional direct voltage reference, $\Delta\hat{E}$, which is determined by a given droop acting on the onshore frequency deviation signal, $\Delta\hat{f}_{\mathrm{on}}$, i.e.

$$\Delta\hat{E} = k_{\mathrm{fE}}\Delta\hat{f}_{\mathrm{on}} \ . \tag{1}$$

$\Delta\hat{f}_{\mathrm{on}}$ is generated by applying a first-order low-pass filter (LPF) and a deadband to the subtraction of the corresponding input signals. Values for the control parameters and limits are given in Table I. Assuming perfect control of the onshore terminal direct voltage, $E_{\mathrm{I}} \approx E_{\mathrm{I}}^{*}$, and perfect estimation of the HVdc link resistance, $\tilde{R}_{\mathrm{dc}} \approx R_{\mathrm{dc}}$,

$$E_{\mathrm{R}} - E_{\mathrm{R}}^{*} = \Delta E_{\mathrm{R}} \approx \Delta\hat{E} = k_{\mathrm{fE}}\Delta\hat{f}_{\mathrm{on}} \ . \tag{2}$$

B. *Offshore Terminal Direct Voltage Estimation*

When the (4 diode bridges of the two 12-pulse) DRs are conducting, the relation between alternating and direct voltages on both sides of the DR platform is [17]

$$E_{\mathrm{R}} = \frac{12\sqrt{6}}{\pi} N_{\mathrm{T_R}} U_{\mathrm{F}} - \frac{12}{\pi} X_{\mathrm{T_R}} I_{\mathrm{R,dc}} \ , \tag{3}$$

where E_{R} is the average direct voltage, $N_{\mathrm{T_R}}$ is the DR transformer turns ratio, U_{F} is the rms line-to-neutral alternating voltage, $X_{\mathrm{T_R}}$ is the DR transformer leakage reactance, and $I_{\mathrm{R,dc}}$ is the direct current flowing out of the DR platform. Moreover, the relation between alternating and direct currents in the DRs (with losses neglected) is [17]

$$I_{\mathrm{R,ac}} \cos\phi \approx \frac{2\sqrt{6}}{\pi} N_{\mathrm{T_R}} I_{\mathrm{R,dc}} \left(1 + \cos\mu\right) \ , \tag{4}$$

where $I_{\mathrm{R,ac}}$ is the rms fundamental alternating line current flowing into the DRs, ϕ is the angle by which the alternating current associated with $I_{\mathrm{R,ac}}$ lags the alternating voltage associated with U_{F}, and μ is the DR commutation overlap angle. Neglecting shunt losses in the DR platform,

$$I_{\mathrm{R,ac}} \cos\phi \approx \frac{P_{\mathrm{F}}}{3\,U_{\mathrm{F}}} \ , \tag{5}$$

where P_{F} is the three-phase active power flowing out of the OWF and into the DR platform. Using (4) and (5), (3) can be rewritten as

$$\begin{aligned} \tilde{E}_{\mathrm{R}} &= \frac{12\sqrt{6}}{\pi} N_{\mathrm{T_R}} U_{\mathrm{F}} - \frac{\sqrt{2/3}\,\tilde{X}_{\mathrm{T_R}}}{N_{\mathrm{T_R}}\left(1+\cos\tilde{\mu}\right)} \frac{P_{\mathrm{F}}}{U_{\mathrm{F}}} \\ &= k_{\mathrm{UE}} U_{\mathrm{F}} - k_{\mathrm{IE}} \frac{P_{\mathrm{F}}}{U_{\mathrm{F}}} \ , \end{aligned} \tag{6}$$

where $\tilde{E}_{\mathrm{R}}$ is the estimated average direct voltage, $\tilde{X}_{\mathrm{T_R}}$ is the estimated DR transformer leakage reactance, and $\tilde{\mu}$ is the estimated DR commutation overlap angle. Equation (6) implies that the offshore terminal direct voltage, E_{R}, can be estimated from measurements local to the OWF, $U_{\mathrm{F}}, P_{\mathrm{F}}$ and knowledge or offline estimation of the parameters corresponding to the DR platform, $N_{\mathrm{T_R}} \tilde{X}_{\mathrm{T_R}}, \tilde{\mu}$. The parameter values used in this work are given in Table II.

If the frequency of the offshore ac network is only allowed to vary within a narrow range around its nominal value (to reduce the size of the filters in the DR platform) [7], the nominal value of the DR transformer leakage reactance, $X_{\mathrm{T_R}}^{\mathrm{nom}}$, can be used in (6), i.e.

$$\tilde{X}_{\mathrm{T_R}} = X_{\mathrm{T_R}}^{\mathrm{nom}} \ . \tag{7}$$

Using (5), (4) can be rewritten as

$$\begin{aligned} \cos\mu &\approx -1 + \frac{\pi}{2\sqrt{6} N_{\mathrm{T_R}}} \frac{I_{\mathrm{R,ac}}}{I_{\mathrm{R,dc}}} \cos\phi \\ &\approx -1 + \frac{\pi}{6\sqrt{6} N_{\mathrm{T_R}}} \frac{P_{\mathrm{F}}}{U_{\mathrm{F}} I_{\mathrm{dc}}} \ . \end{aligned} \tag{8}$$

Using (8), $\cos\mu$ can be estimated from measurements for different operating points. $\tilde{\mu}$ can then be calculated as

$$\tilde{\mu} = \arccos\left(\overline{\cos\mu}\right) \ , \tag{9}$$

where $\overline{\cos\mu}$ is the mean of the estimated values for $\cos\mu$.

C. *Wind Turbine Front-End Converter Controls*

The front-end (line-side) network of the kth wind turbine(s), WT_k, is shown in Fig. 3. The grid-forming WT front-end (line-side) converter (FEC) controls, described in [12], are based on those proposed in [6] and are implemented on a rotating reference frame oriented on the voltage at the filter capacitor, $U_{\mathrm{T},k}$.

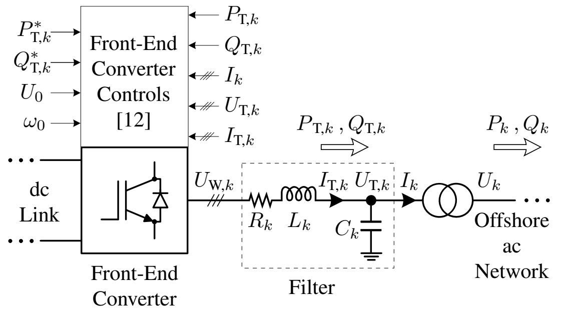

Fig. 3. kth wind turbine front-end (line-side) network

D. Wind Farm Active Power Control

To study the capability of such a WF to provide FS to an onshore ac network, the model is extended to include the supervisory active power control at plant level shown in Fig. 4, based on those used in [11], [12], [16]. Values for the parameters and limits are given Table III.

In the right side of Fig. 4, a proportional-integral (PI) regulator controls the WF active power output, P_{F}, by altering the WF active power dispatch, P^*. A first-order LPF is applied to the corresponding measurement signal. Hardware and control limits are modelled by means of corresponding restrictions on the regulator's output value and its rate of change. Proportional WF generation dispatch is used. In doing so, P^* is divided by the overall aerodynamic power available from the wind, P_{ava}, to generate the OWF active power dispatch coefficient, κ_{disp}. The active power set point of each WT FEC is then set as the product of the corresponding aerodynamic power available from the wind, $P_{\mathrm{ava},k}$, and the active power dispatch coefficient, i.e.

$$P^*_{\mathrm{T},k} = \kappa_{\mathrm{disp}} P_{\mathrm{ava},k} \ . \tag{10}$$

When providing FS to the onshore ac network, the base active power reference, P^*_{F}, is modified by means of an additional active power reference, ΔP_{FS}, based on an onshore frequency deviation signal, $\Delta \check{f}_{\mathrm{on}}$, i.e.

$$\check{P} = P^*_{\mathrm{F}} + \Delta P_{\mathrm{FS}}(\Delta \check{f}_{\mathrm{on}}) \ . \tag{11}$$

PFR is implemented by making ΔP_{FS} proportional to $\Delta \check{f}_{\mathrm{on}}$ (to which a first-order LPF and a deadband can also be applied), using a given droop.

When providing CLFS, $\Delta \check{f}_{\mathrm{on}}$ is determined by applying a given droop to the offshore (terminal) direct voltage deviation signal, $\Delta \check{E}_{\mathrm{R}}$. Assuming perfect knowledge of the offshore terminal direct voltage, $\Delta \check{E}_{\mathrm{R}} \approx \Delta E_{\mathrm{R}}$,

$$\Delta \check{f}_{\mathrm{on}} = k_{\mathrm{Ef}} \Delta \check{E}_{\mathrm{R}} \approx k_{\mathrm{Ef}} \Delta E_{\mathrm{R}} \ . \tag{12}$$

Equations (2) and (12) can be combined as:

$$\Delta \check{f}_{\mathrm{on}} \approx k_{\mathrm{Ef}} k_{\mathrm{fE}} \Delta \hat{f}_{\mathrm{on}} = \Delta f_{\mathrm{on}} \iff k_{\mathrm{Ef}} k_{\mathrm{fE}} = 1 \ , \tag{13}$$

which implies that the onshore frequency deviation signal, $\Delta \hat{f}_{\mathrm{on}}$, can be estimated in the WF active power control scheme without any need for long-distance communication. The choice of values for k_{Ef} and k_{fE} must ensure that the direct voltage variations due to onshore frequency deviations are sufficiently large to be distinguishable from normal voltage drifts and measurement and estimation uncertainty, but sufficiently small to lie within the allowable operating range. By applying the corresponding deadbands, the controls can ignore small deviations in onshore frequency or offshore terminal direct voltage.

Two different methods are proposed for implementing CLFS in the WF active power controls. In Method 1 (CLFS$_1$), shown in Fig. 4, the estimated offshore terminal direct voltage (6), $\tilde{E}_{\mathrm{R}}$, is used for computing $\Delta \check{E}_{\mathrm{R}}$. In Method 2 (CLFS$_2$), the actual offshore terminal direct voltage measurement, E_{R}, is used instead of $\tilde{E}_{\mathrm{R}}$.

III. Simulation Results

Results of the performed dynamic simulations are presented in Figs. 5–10. The results illustrated in Figs. 5–8, discussed in Section III-A correspond to the closed-loop tests conducted to assess the dynamic performance of the proposed CLFS methods and compare it with that of CBFS. Figs. 9 and 10, discussed in Section III-B, correspond to the parametric sensitivity study conducted to asses the proposed CLFS methods' accuracy and sensitivity to parameter estimation errors.

Onshore frequency events have been simulated by means of a $0.075\,\mathrm{pu}$ load step change (i.e. $60\,\mathrm{MW}/800\,\mathrm{MW}$) at $t = 0.5\,\mathrm{s}$ for different wind speed scenarios over the whole OWF's operating range. Wind speed (and the aerodynamic power available from it) has been considered constant in each simulation. All (equivalent) WT front-end networks and corresponding grid-forming converter controls have the same parameter per-unit (pu) values. Moreover, the offshore ac network voltage magnitude and (angular) frequency set points, U_0 and ω_0, respectively, and the FEC reactive power references, $Q^*_{\mathrm{T},k}$, are $U_0 = 0.86\,\mathrm{pu}$, $\omega_0 = 1\,\mathrm{pu}$, $Q^*_{\mathrm{T},k} = 0$ for all WTs, and $f^*_{\mathrm{on}} = 1\,\mathrm{pu} = E^*_{\mathrm{R}}$ in the controls depicted in Figs. 2 and 4. A maximum allowable variation of $0.06\,\mathrm{pu}$ ($2\,\%$ of the HVdc link's rated voltage) has been assumed for E_{R}.

A. Closed-Loop Performance

Results of the closed-loop tests are shown in Figures 5–8. Each fig. includes base case responses, corresponding to no FS from the OWF to the onshore ac network (i.e. the FS consisting solely of that of the SM). The (light) grey signals in each fig. represent the base case, while the (dark) red and black traces illustrate the cases in which the OWF provides CBFS and CLFS, respectively. In the case with CBFS, $\Delta \hat{f}_{\mathrm{on}}$ has been assumed to be communicated continuously to the OWF with a delay of $100\,\mathrm{ms}$. Method 1 (CLFS$_1$) has been employed in the case with CLFS. The dynamic performance of the case using CLFS$_2$ is almost identical to that of the case employing CLFS$_1$ and is thus omitted.

High, medium and low wind speed scenarios have been considered in these tests. As with those in [12], the considered individual WT operating points in each scenario take into account the wind speed deficit due to the aerodynamic interaction between WTs. In principle, $P_{\mathrm{ava},k}$ decreases along the string in the wind speed direction.WF production is curtailed preventively to provide active power reserves of $0.1\,\mathrm{pu}$, i.e. $P^*_{\mathrm{F}} = P_{\mathrm{ava}} - 0.1\,\mathrm{pu}$.

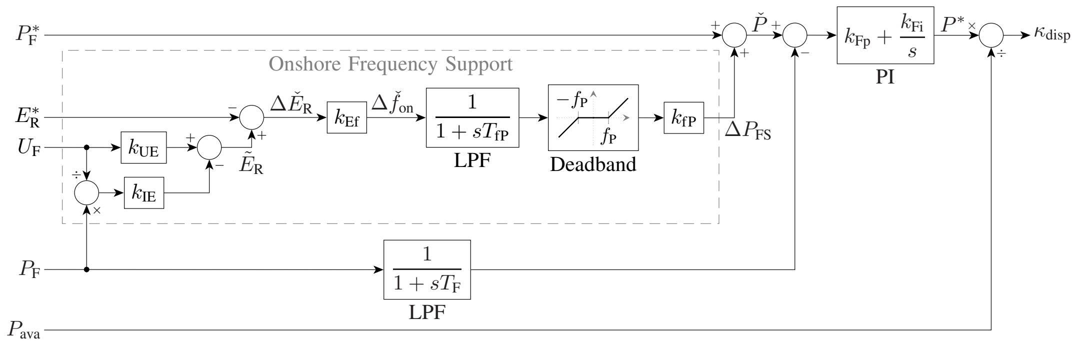

Fig. 4. Wind farm active power control using CLFS_1; parameter values and limits given in Table III

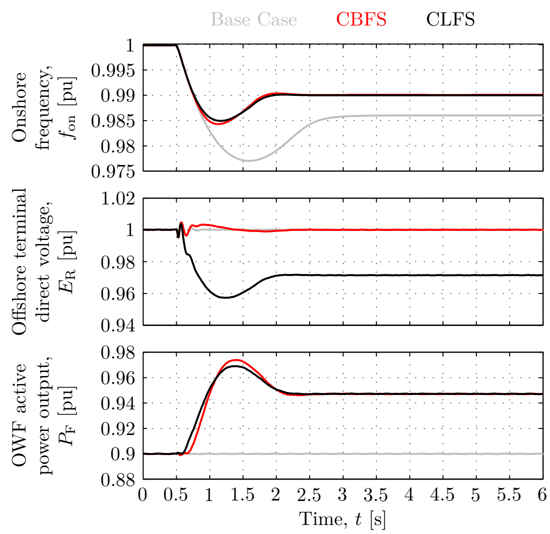

(a)

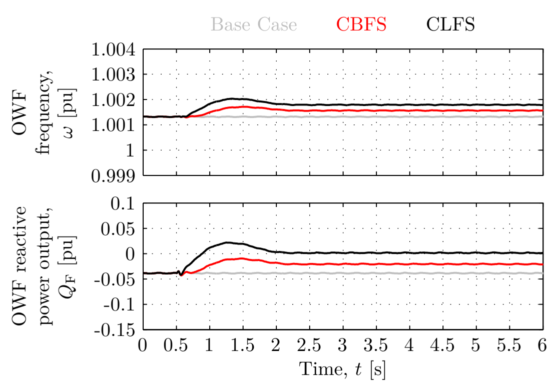

(b)

Fig. 5. Wind farm response to an onshore underfrequency event at high wind speed

WF responses to an onshore underfrequency event at high and low wind speeds are depicted in Figs. 5 and 6, respectively. Similar results have been obtained in the medium wind speed scenario. The offshore ac network (angular) frequency, ω, and WF reactive power output, Q_F, are only presented in Fig. 5b, corresponding to the high wind speed scenario. However, similar results have also been obtained in the other wind speed scenarios.

As can be seen in Figs. 5 and 6, the onshore frequency

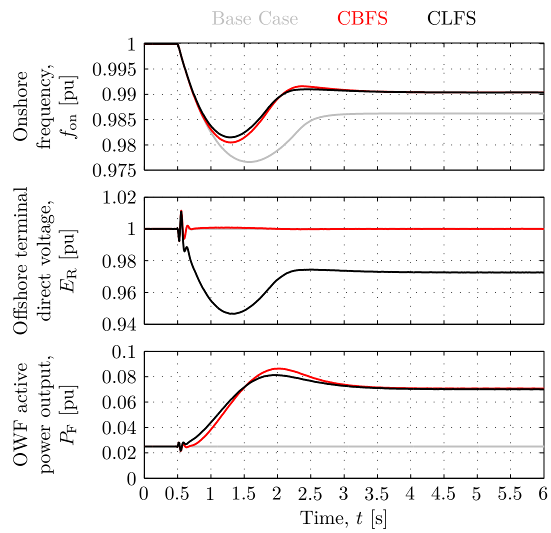

Fig. 6. Wind farm response to an onshore underfrequency event at low wind speed

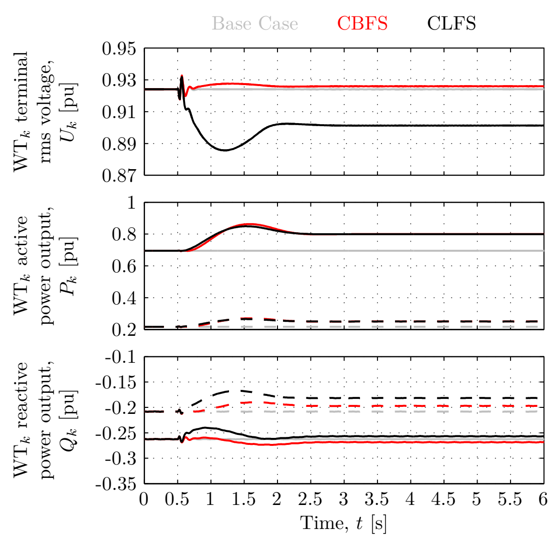

Fig. 7. kth wind turbine response to an onshore underfrequency event at medium-low wind speed – Solid: $k = 1$, Dashed: $k = 9$

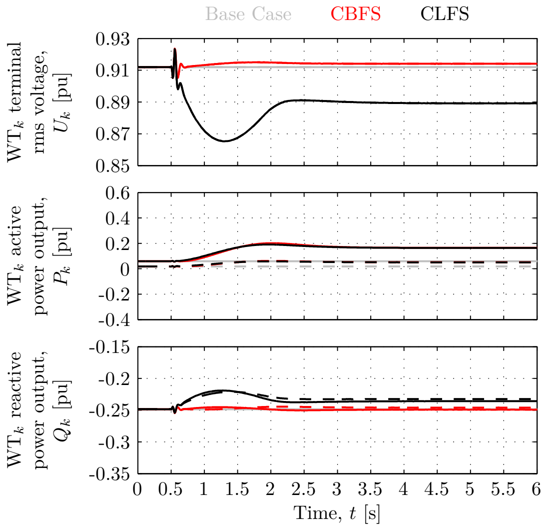

Fig. 8. kth wind turbine response to an onshore underfrequency event at low wind speed – Solid: $k = 1$, Dashed: $k = 9$

response can be improved by having the OWF provide FS to the onshore ac network: by drawing on the active power reserves and increasing P_{F}, the OWF increases f_{on} and maintains it at a higher value for as long as the wind allows. An increase in P_{F} results in an increase in the DR reactive power consumption. This is reflected in the increases in Q_{F} and ω in Fig. 5b. However, such changes are one and three orders of magnitude smaller than that in P_{F}, respectively, while ω is kept close to 1 pu. That is the result of every grid-forming WT FEC contributing autonomously to regulating ω by means of its corresponding PLL-based proportional (P) controller, while sharing the reactive power with the other grid-forming WT FECs by means of its reactive-power-frequency droop (P regulator).

WT responses to an onshore underfrequency event at medium and low wind speeds are illustrated by Figs. 7 and 8, respectively. Solid and dashed traces—superimposed in the case of the WT terminal rms voltages, U_k—represent the responses of WTs 1 and 9, respectively, corresponding to the turbines at both ends of the string that is represented in detail. Similar results have been obtained in the high wind speed scenario.

The WT active power outputs, P_k, in Figs. 7 and 8 reflect the assumed distributions of $P_{\mathrm{ava},k}$ and the changes in P^* and κ_{disp} when FS is provided. In all wind speed scenarios, the increase in P_{F} in response to the onshore underfrequency event is achieved by an increase in U_k that is one order of magnitude smaller, keeping them within their normal operating range, as depicted in both figs. As shown also in both figs., the WTs share the reactive power consumption (negative values of Q_k) according to their power rating and their active power output, P_k.

Unique features of the provision of CLFS from OWFs connected to HVdc via DRs are illustrated by the traces of ω and U_{k} in Figs. 5b, 7 and 8:

- Since the DRs clamp the magnitude of the alternating voltage in the offshore ac network to the offshore terminal direct voltage, changes in the latter are naturally reflected in the former, without the need of an additional control loop.
- The onshore frequency is not mirrored in the offshore ac network, but its deviation is reflected in the magnitude of the alternating voltage in the offshore ac network.
- The OWF active power controls can use the magnitude of the alternating voltage in the offshore ac network—instead of its frequency—to estimate the active power imbalance in the onshore ac network.
- Since the voltage drop over the DRs varies with the operating point, an accurate provision of CLFS over the whole operating range of the OWF requires knowledge of either the offshore terminal direct voltage or the OWF operating point (e.g. OWF active power or current output).

The overall performance of the case with CLFS is very similar to that of the case with CBFS, as evidenced by the traces of f_{on} and P_{F} in Figs. 5 and 6. A similar amount of energy is injected in both cases, but it is injected at different rates. The dynamic performance of the case with CLFS is slightly better immediately after the event, as the onshore terminal extracts active power from the HVdc link to lower its voltage, and slightly worse after the frequency nadir, as some of the OWF active power output is used to raise such voltage. Such behaviour is, in general, preferable, as the faster response immediately after the event assists in limiting the nadir, while the slower response occurs after the most critical stage of the event has passed. The slightly worse static performance (i.e. smaller steady-state values of f_{on} and P_{F}) can be attributed mainly to the error in the estimation of E_{R}.

As illustrated by Fig. 5, the consumption/production of reactive power, necessary to control the offshore ac network (angular) frequency, ω, can reduce the active power headroom of the corresponding grid-forming WTs. Lowering the voltage in response to an onshore underfrequency event may thus require a greater WT FEC current headroom to provide the necessary additional active power at high wind speeds. Moreover, there is a trade-off at low wind speeds between the maximum allowable variation of E_{R} and the minimum allowable WT terminal voltage, U_k, as can be observed in Fig. 8, e.g. increasing the variation of E_{R} may result in values of U_k below 0.85 pu.

B. Accuracy and Sensitivity to Parameter Estimation Errors

To assess the impact of parameter estimation errors (i.e. in the estimation of $\tilde{R}_{\mathrm{dc}}$ in both methods, plus $\tilde{\mu}$ and $\tilde{X}_{\mathrm{T_R}}$ in CLFS$_1$) on the provision of CLFS, a parametric sensitivity study has been performed, with the results shown in Figs. 9 and 10. The study has consisted of open-loop tests, in which the onshore terminal modulates the HVdc link voltage in proportion to the onshore frequency deviation (1), but the OWF does not provide FS to the onshore ac network, i.e. the OWF active power output, P_{F}, remains constant. The same aerodynamic power available from the wind has been considered for all WTs. Moreover, no active power reserves from preventively curtailed OWF production have been considered, i.e. $P_{\mathrm{F}}^* = P_{\mathrm{ava}}$.

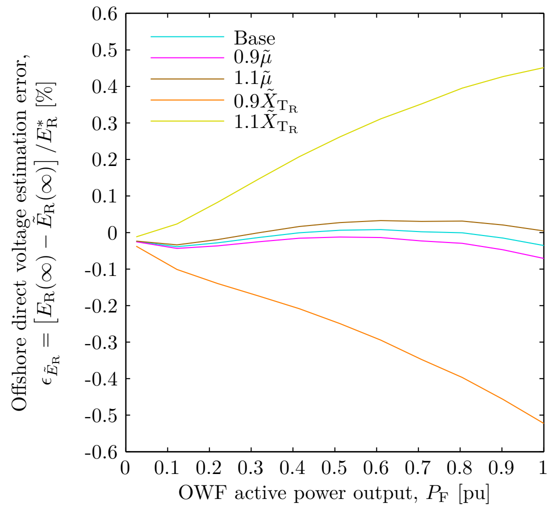

Fig. 9. Parametric sensitivity analysis of the offshore direct voltage estimation

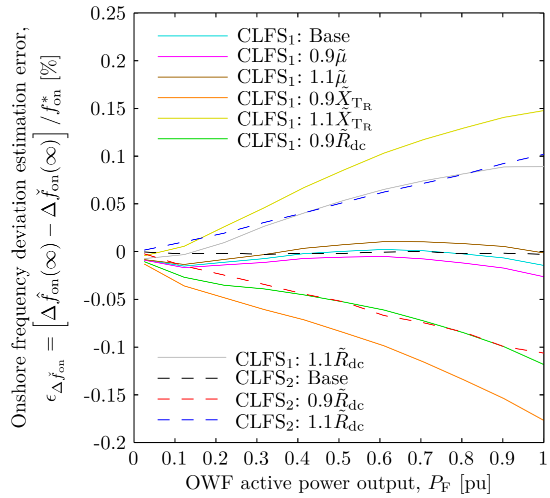

Fig. 10. Parametric sensitivity analysis of the onshore frequency deviation estimation

The plots represent the steady-state values of different quantities from the dynamic simulations of onshore underfrequency events similar to those in Section III-A, for different operating points (i.e. OWF active power output, P_{F}) in the OWF operating range. Moreover, they include base cases, corresponding to $\tilde{R}_{\mathrm{dc}} \approx R_{\mathrm{dc}}$ and the recommended estimation of $\tilde{X}_{\mathrm{T_R}}$ and $\tilde{\mu}$, (7), (9). The corresponding values are given in Tables I and II. The onshore underfrequency events have been arranged so that the steady-state value of the onshore frequency deviation signal, $\Delta\hat{f}_{\mathrm{on}}(\infty)$, has a magnitude of about $0.0136\,\mathrm{pu}$ (e.g. $0.68\,\mathrm{Hz}$ for $f^*_{\mathrm{on}} = 50\,\mathrm{Hz}$) in every simulation. However, similar results can be expected over the assumed ranges for onshore frequency deviation signal and offshore direct voltage, $\Delta\hat{f}_{\mathrm{on}} \in [-0.02, 0.02]\,\mathrm{pu}$, $E_{\mathrm{R}} \in [0.94, 1.06]\,\mathrm{pu}$.

Fig. 9 illustrates the accuracy of the offshore terminal direct voltage estimation (6), $\tilde{E}_{\mathrm{R}}$, used in CLFS$_1$, and its sensitivity to errors in the estimation of $\tilde{X}_{\mathrm{T_R}}$ and $\tilde{\mu}$. This is done by representing the error of $\tilde{E}_{\mathrm{R}}$, $\epsilon_{\tilde{E}_{\mathrm{R}}} = (E_{\mathrm{R}} - \tilde{E}_{\mathrm{R}})/E^*_{\mathrm{R}}$, for the base case parameter values and variations of $\pm 10\,\%$. Variations in $\tilde{R}_{\mathrm{dc}}$ have a negligible effect on $\epsilon_{\tilde{E}_{\mathrm{R}}}$ (i.e. they are reflected in both terms of the subtraction) and are thus omitted.

Fig. 10 depicts the accuracy of the onshore frequency deviation estimation (12), $\Delta\check{f}_{\mathrm{on}}$, and its sensitivity to errors in the estimation of $\tilde{R}_{\mathrm{dc}}$, $\tilde{X}_{\mathrm{T_R}}$ and $\tilde{\mu}$ for both CLFS methods. This is done by representing the error of $\Delta\check{f}_{\mathrm{on}}$, $\epsilon_{\Delta\check{f}_{\mathrm{on}}} = (\Delta\hat{f}_{\mathrm{on}} - \Delta\check{f}_{\mathrm{on}})/f^*_{\mathrm{on}}$, for the base case parameter values and for variations of $\pm 10\,\%$. The solid traces represent the cases with CLFS$_1$, while the dashed traces correspond to the cases with CLFS$_2$. Variations in $\tilde{X}_{\mathrm{T_R}}$ and $\tilde{\mu}$ are only relevant to CLFS$_1$ and are thus omitted for CLFS$_2$.

As evidenced by the cyan (base case) trace in Fig. 9, the results indicate that the proposed method (6) for estimating E_{R} can be expected to have an error, $\epsilon_{\tilde{E}_{\mathrm{R}}}$, of around $0.03\,\%$ in magnitude (i.e. $64\,\mathrm{V}$ for $E^*_{\mathrm{R}} \approx 213\,\mathrm{kV}$), which may be inherent to any estimation of E_{R}. As a consequence, $\epsilon_{\Delta\check{f}_{\mathrm{on}}}$ can be expected to be around 0.01 percentage points (e.g. $5\,\mathrm{mHz}$ for $f^*_{\mathrm{on}} = 50\,\mathrm{Hz}$) greater when using CLFS$_1$, as illustrated by the cyan and black (base case) curves in Fig. 10. Variations in $\tilde{R}_{\mathrm{dc}}$, $\tilde{X}_{\mathrm{T_R}}$ and $\tilde{\mu}$ impact the estimations of offshore direct voltage and onshore frequency deviation in a manner that is directly proportional to P_{F}, as can be seen in both figs. This reflects the role of such parameters in the estimation of the corresponding voltage drops in the DR platform and HVdc link, which are directly proportional to P_{F}. The maximum values of $\epsilon_{\tilde{E}_{\mathrm{R}}}$ and $\epsilon_{\Delta\check{f}_{\mathrm{on}}}$ thus correspond to $P_{\mathrm{F}} = 1\,\mathrm{pu}$.

When using CLFS$_1$, an error of $\pm 10\,\%$ in the estimation of $\tilde{\mu}$ can result in greater magnitudes of $\epsilon_{\tilde{E}_{\mathrm{R}}}$ and $\epsilon_{\Delta\check{f}_{\mathrm{on}}}$, as depicted by the magenta and brown traces in Figs. 9 and 10, respectively. Such magnitudes can be as high as $0.06\,\%$ and $0.02\,\%$, respectively. Likewise, an error of $\pm 10\,\%$ in the estimation of $\tilde{X}_{\mathrm{T_R}}$ can result in magnitudes of $\epsilon_{\tilde{E}_{\mathrm{R}}}$ and $\epsilon_{\Delta\check{f}_{\mathrm{on}}}$ as high as $0.52\,\%$ and $0.17\,\%$, respectively, as illustrated by the orange and yellow curves in Figs. 9 and 10, respectively.

An error of $\pm 10\,\%$ in the estimation of $\tilde{R}_{\mathrm{dc}}$ can result in magnitudes of $\epsilon_{\Delta\check{f}_{\mathrm{on}}}$ as high as $0.12\,\%$, which indicates that $\epsilon_{\Delta\check{f}_{\mathrm{on}}}$ is more sensitive to errors in the estimation of $\tilde{R}_{dc}$ than to errors in the estimation of $\tilde{\mu}$, but is even more sensitive to errors in the estimation of $\tilde{X}_{\mathrm{T_R}}$. As illustrated by the red and blue curves, the $\pm 10\,\%$ error in the estimation of $\tilde{R}_{\mathrm{dc}}$ has a similar effect on $\epsilon_{\Delta\check{f}_{\mathrm{on}}}$ when using CLFS$_2$. Moreover, similar accuracy and sensitivity to errors in the estimation of $\tilde{R}_{\mathrm{dc}}$ can be expected when VSC-connected OWFs provide CLFS.

In OWFs, transformers are typically purpose-built, meaning that the uncertainty in the estimation of $\tilde{X}_{\mathrm{T_R}}$ can be reduced significantly by measuring their impedance during acceptance tests. The uncertainty in the estimation of $\tilde{R}_{\mathrm{dc}}$ can be reduced by the distributed temperature sensing systems typically employed in large OWFs. Since the corresponding thermal time constants are much greater, corrections in $\tilde{R}_{\mathrm{dc}}$ can be done at a lower frequency, e.g. every 10 minutes. Moreover, adaptive estimators can also be used to correct the values of $\tilde{\mu}$, $\tilde{X}_{\mathrm{T_R}}$ and $\tilde{R}_{\mathrm{dc}}$ at similar frequencies.

IV. Conclusions

The simulation results indicate that the new connection concept using DRs (and corresponding changes in WT control) does not impact the capability of OWFs to provide CLFS by means of plant-level active power control strategies similar to those developed for OWFs connected to HVdc via VSCs. The onshore frequency is not mirrored in the offshore ac network, but its deviation is reflected in the magnitude of the alternating voltage in the offshore ac network, while the offshore frequency varies relatively little. The proposed OWF active power controls can use the magnitude of the alternating voltage in the offshore ac network—instead of its frequency—to estimate the active power imbalance in the onshore ac network. In this way, DR-connected OWFs respond to onshore frequency events, while their grid-forming WTs share the reactive power consumption/production and keep the offshore frequency and voltages within their normal operating ranges.

The overall performance of the case with CLFS is similar to that of the case with CBFS. The dynamic performance is slightly better immediately after the event, as the onshore terminal extracts active power from the HVdc link to lower its voltage, and slightly worse after the frequency nadir, as some of the OWF active power output is used to raise such voltage. Such behaviour is, in general, preferable, as the faster response immediately after the event assists in limiting the nadir, while the slower response occurs after the most critical stage of the event has passed.

Appendix

TABLE I
ONSHORE TERMINAL OUTER CONTROL LOOP PARAMETERS AND LIMITS

Par.	Value	Par.	Value
f_{E}	$5 \times 10^{-4}\,\mathrm{pu}$	$\tilde{R}_{\mathrm{dc}}$	$3.05 \times 10^{-2}\,\mathrm{pu}$
k_{fE}	$3\,\mathrm{pu}$	T_{fE}	$10\,\mathrm{ms}$
Limits:	$-0.06\,\mathrm{pu} \leq \Delta\hat{E} \leq 0.06\,\mathrm{pu}$		

TABLE II
OFFSHORE TERMINAL DIRECT VOLTAGE ESTIMATION PARAMETERS

Par.	Value	Par.	Value	Par.	Value
$\tilde{\mu}$	$22.3°$	$N_{\mathrm{T_R}}$	$43.37/66$	$\tilde{X}_{\mathrm{T_R}}$	$1.41\,\Omega$

TABLE III
WIND FARM ACTIVE POWER CONTROL PARAMETERS AND LIMITS

Par.	Value	Par.	Value	Par.	Value
f_{P}	0	k_{Fp}	$1 \times 10^{-3}\,\mathrm{pu}$	k_{UE}	$1.10\,\mathrm{pu}$
k_{Ef}	$0.333\,\mathrm{pu}$	k_{Fi}	$5\,\mathrm{pu/s}$	T_{F}	$10\,\mathrm{ms}$
k_{fP}	$-5\,\mathrm{pu}$	k_{IE}	$4.48 \times 10^{-2}\,\mathrm{pu}$	T_{fP}	$10\,\mathrm{ms}$
Limits:	$1 \times 10^{-3}\,\mathrm{pu} \leq U_{\mathrm{F}}$, $1 \times 10^{-3}\,\mathrm{pu} \leq P_{\mathrm{ava}}$, $-0.1\,\mathrm{pu} \leq \Delta P_{\mathrm{FS}} \leq 0.1\,\mathrm{pu}$, $0.025\,\mathrm{pu} \leq P^{*} \leq 1.1\,\mathrm{pu}$, $-1\,\mathrm{pu/s} \leq \mathrm{d}P^{*}/\mathrm{d}t \leq 1\,\mathrm{pu/s}$				

Acknowledgement

The authors gratefully acknowledge the contributions of Poul E. Sørensen to the discussions leading up to this work.

References

[1] R. M. Blasco-Giménez, S. C. Añó-Villalba, J. Rodríguez-D'Derlée, F. Morant-Anglada, and S. I. Bernal-Pérez, "Distributed Voltage and Frequency Control of Offshore Wind Farms Connected With a Diode-Based HVdc Link," *IEEE Transactions on Power Electronics*, vol. 25, no. 12, pp. 3095–3105, Dec. 2010.

[2] R. M. Blasco-Giménez, S. C. Añó-Villalba, J. Rodríguez-D'Derlée, S. I. Bernal-Pérez, and F. Morant-Anglada, "Diode-Based HVdc Link for the Connection of Large Offshore Wind Farms," *IEEE Transactions on Energy Conversion*, vol. 26, no. 2, pp. 615–626, Mar. 2011.

[3] S. I. Bernal-Pérez, S. C. Añó-Villalba, R. M. Blasco-Giménez, and J. Rodríguez-D'Derlée, "Efficiency and Fault Ride-Through Performance of a Diode-Rectifier- and VSC-Inverter-Based HVDC Link for Offshore Wind Farms," *IEEE Transactions on Industrial Electronics*, vol. 60, no. 6, pp. 2401–2409, Jun. 2013.

[4] T. Christ, S. Seman, and R. Zurowski, "Investigation of DC Converter Nonlinear Interaction with Offshore Wind Power Park System," in *Proceedings of the 2015 EWEA Offshore Conference*, Copenhagen, Denmark, 10th–12th Mar. 2015.

[5] P. Menke, R. Zurowski, T. Christ, S. Seman, G. Giering, T. Hammer, W. Zink, F. Hacker, D. Imamovic, J. Thisted, P. Brogan, and N. Goldenbaum, "2nd Generation DC Grid Access for Large Scale Offshore Wind Farms," in *Proceedings of the 14th Wind Integration Workshop*, Brussels, Belgium, 20th–22nd Oct. 2015.

[6] L. Yu, R. Li, and L. Xu, "Distributed PLL-Based Control of Offshore Wind Turbines Connected With Diode-Rectifier-Based HVDC Systems," *IEEE Transactions on Power Delivery*, vol. 33, no. 3, pp. 1328–1336, Jun. 2018.

[7] PROMOTioN, "Deliverable 3.1: Detailed functional requirements to WPPs," Project Deliverable, Dec. 2016. [Online]. Available: https://www.promotion-offshore.net/fileadmin/PDFs/D3.1_PROMOTioN_Deliverable_3.1_Detailed_functional_requirements_to_WPPs.pdf.

[8] L. Fan, Z. Miao, and D. Osborn, "Wind Farms With HVDC Delivery in Load Frequency Control," *IEEE Transactions on Power Systems*, vol. 24, no. 4, pp. 1894–1895, Nov. 2009.

[9] Y. Pipelzadeh, B. Chaudhuri, and T. C. Green, "Inertial Response from Remote Offshore Wind Farms Connected Through VSC-HVDC Links: A Communication-less Scheme," in *Proceedings of the IEEE PES 2012 General Meeting*, San Diego, CA, United States, 22nd–26th Jul. 2012.

[10] Y. Phulpin, "Communication-Free Inertia and Frequency Control for Wind Generators Connected by an HVDC-Link," *IEEE Transactions on Power Systems*, vol. 27, no. 2, pp. 1136–1137, May 2012.

[11] PROMOTioN, "Deliverable 3.5: Performance of ancillary services provision from WFs connected to DR-HVDC," Project Deliverable, Jan. 2018. [Online]. Available: https://www.promotion-offshore.net/fileadmin/PDFs/D3.5_PROMOTioN_Performance_of_ancillary_services_provision_from_WFs_connected_to_DR-HVDC.pdf.

[12] O. Saborío-Romano, A. Bidadfar, J. N. Sakamuri, Ö. Göksu, and N. A. Cutululis, "Primary Frequency Response from Offshore Wind Farms Connected to HVdc via Diode Rectifiers," in *Proceedings of the 13th IEEE PES PowerTech Conference*, Milan, Italy, 23rd–27th Jun. 2019.

[13] PROMOTioN, "Deliverable 3.2: Specifications of the control strategies and the simulation test cases," Project Deliverable, Mar. 2017. [Online]. Available: https://www.promotion-offshore.net/fileadmin/PDFs/D3.2_Specifications_Control_strategies_and_simulation_test_cases.pdf.

[14] L. Xie, L. Yao, Y. Li, L. Xu, Z. Wang, C. Wei, and C. Fan, "Frequency regulation participation of offshore wind farm integrated by diode-rectifer HVDC system," *The Journal of Engineering*, vol. 2019, pp. 977–981, 16 Apr. 2019.

[15] E. Muljadi, S. Pasupulati, A. Ellis, and D. Kosterov, "Method of Equivalencing for a Large Wind Power Plant with Multiple Turbine Representation," in *Proceedings of the IEEE PES 2008 General Meeting*, Pittsburgh, PA, United States, 20th–24th Jul. 2008.

[16] L. Zeni, "Power system integration of VSC-HVDC connected wind power plants: Control principles, power system services, clustering of wind power plants," PhD thesis, Technical University of Denmark, Roskilde, Denmark, Mar. 2015.

[17] P. Kundur, *Power System Stability and Control*. New York, NY, United States: McGraw-Hill, 1994.